Chemical Physics 397 (2012) 74–81

Contents lists available at SciVerse ScienceDirect

Chemical Physics

journal homepage: www.elsevier.com/locate/chemphys

Autoionization rate constants of zero electron kinetic energy Rydberg states

H. Mineo [a], Y.H. Wang [a], S.D. Chao [a,*], S.H. Lin [b,c]

[a] Institute of Applied Mechanics, National Taiwan University, Taipei 106, Taiwan, ROC
[b] Department of Applied Chemistry, National Chiao-Tung University, Hsin-Chu 300, Taiwan, ROC
[c] Institute of Atomic and Molecular Sciences, Academia Sinica, Taipei 106, Taiwan, ROC

ARTICLE INFO

Article history:
Received 5 October 2011
In final form 10 January 2012
Available online 3 February 2012

Keywords:
Density matrix method
Inverse Born–Oppenheimer approximation
Zero electron kinetic energy (ZEKE) spectroscopy
Autoionization
Rydberg states

ABSTRACT

We have calculated the vibrational and rotational autoionization rate constants for diatomic molecules H_2, N_2, and HCl in high Rydberg states by employing the density matrix formulation with the inverse Born–Oppenheimer approximation basis set. The purpose is to simulate the main radiationless processes occurring in zero electron kinetic energy (ZEKE) spectroscopy. The quantum numbers and the energy dependences of the calculated autoionization rate constants are represented as the scaling laws via non-linear regression. These data provide a suitable starting point for quantitative study of the intricate dynamics involved in ZEKE Rydberg states.

1. Introduction

Zero electron kinetic energy (ZEKE) spectroscopy is a very high resolution photoelectron spectroscopy (PES) for studying the structures and dynamics of neutral and ionic molecules [1–4]. It has been routinely used to determine the rovibronic energy levels of polyatomic molecular ions and to obtain information on the dynamical and thermodynamical properties of molecular systems [4–10]. Moreover, several new laser spectroscopy methods, such as mass analyzed threshold ionization (MATI) spectroscopy [11], threshold ion-pair production spectroscopy (TIPPS) [12], and the Rydberg-tagging time-of-flight (RTTOF) method [13] employ detection concepts similar to that used in ZEKE spectroscopy. This has stimulated considerable interest in understanding of the behavior of molecules with energies very close to their ionization thresholds. The central point in understanding the observed ZEKE spectra, which underpins the success of ZEKE techniques, is the intricate dynamics of very high Rydberg states with a principal quantum number $n = 100$ or more. The study of high Rydberg states represents a huge extension of the conventional spectroscopy and dynamics of ground states and low electronically excited states. However, in contrast to the latter, high Rydberg dynamics exhibits special characteristics, which have been difficult to interpret using familiar principles applicable for low-lying states.

In a ZEKE experiment, a laser pulse will excite the molecule to a high Rydberg state just beneath the ionization threshold. Upon the excitation, many radiative and radiationless processes occur. These include spontaneous emission, autoionization, field induced ionization and channel coupling. Then the electrons would be detected by using a delayed ionizing field. Different from the conventional photoelectron spectroscopy, which directly detects electrons in the continuum states, in ZEKE spectroscopy the electrons from the high Rydberg states are observed [14,15]. For this reason, it is crucial to find a suitable representation of the high Rydberg state for studying the involved radiative and radiationless processes. The optically pumped state is described as a high n Rydberg electronic state where classically the electron moves relatively slower than the nuclear motion of the parent ion. In this case, the Rydberg electronic energy levels are even smaller than the rovibrational energy levels of the ion. This classical picture motivates the concept of the inverse Born–Oppenheimer approximation (IBOA) [16–18] and using the IBOA we can establish a proper basis set for the study of ZEKE/MATI spectra [19,20].

Because the measurements of ZEKE spectra consist of a series of processes, the density matrix formulation is a proper technique to start. The master equations (MEs) can be derived for each process and can be solved sequentially given proper experimental conditions such as frequencies, intensities, pulse duration of the pumping laser, and the time-durations of l-mixing, discrimination field and extraction fields. By solving this series of MEs we obtain not only the intensity of ZEKE electrons associated with the ZEKE spectra but the insight into the most detailed dynamics associated with these states.

In this paper, we present the master equation for autoionization dynamics based on the inverse Born–Oppenheimer approximation.

* Corresponding author.
E-mail address: sdchao@iam.ntu.edu.tw (S.D. Chao).

0301-0104/$ - see front matter © 2012 Elsevier B.V. All rights reserved.
doi:10.1016/j.chemphys.2012.01.002

With such approach we calculate the autoionization rates constants for both vibrationally and rotationally radiationless transitions among ZEKE Rydberg states. In Section 2, we outline the necessary theoretical formulations and in Section 3 we show the numerical calculation of autoionization rate constants and the related scaling laws. A brief summary is given in Section 4.

2. Theory

We use the stochastic Liouville equation [20]

$$\frac{d\hat{\rho}}{dt} = -\frac{i}{\hbar}[\hat{H}, \hat{\rho}] - \hat{\Gamma}\hat{\rho} \tag{2.1}$$

where $\hat{H}$ and $\hat{\rho}$ represent the molecular Hamiltonian and the density matrix of the molecule, respectively, and $\hat{\Gamma}$ denotes the damping operator. The diagonal (off-diagonal) matrix elements of $\hat{\rho}$ represent the population (coherence or phase) of the molecule. Autoionization can be described as the transition from a ZEKE Rydberg state of the higher ionization potential (IP) to the ionization continuum of the lower IP [21,22]. For the ZEKE states (represented by m) and the ionization continuum (represented by k), using the Markoff approximation [23], Eq. (2.1) becomes

$$\frac{d\rho_{mm}}{dt} = -W_m\rho_{mm}(t) - \gamma_m\rho_{mm}(t) \tag{2.2}$$

where $\hat{H}'$ is the interaction responsible for the autoionization, $\gamma_m = \Gamma_{mm}^{mm}$ represents the radiative rate constant, and

$$W_m = \frac{2}{\hbar^2}\sum_k |H'_{km}|^2 D(\omega_{mk}) \tag{2.3}$$

denotes the autoionization rate constant and $D(\omega_{mk})$ denotes the Lorentzian

$$D(\omega_{mk}) = \frac{1}{\pi}\frac{\gamma_m/2}{\omega_{mk}^2 + (\gamma_m/2)^2} \tag{2.4}$$

Although usually the population components are observed, using short excitation laser-pulse, the quantum beat can also be observed in ZEKE spectroscopy [24].

Using the inverse Born–Oppenheimer approximation (IBOA) [16–18], the molecular Hamiltonian can be expressed as

$$\hat{H} = \hat{H}_{ion} + \hat{T}_e \tag{2.5}$$

where $\hat{H}_{ion}$ is the ionic Hamiltonian and $\hat{T}_e$ denotes the kinetic energy operator of the Rydberg electron. We first neglect the $\hat{T}_e$ term, and solve the ionic Schrödinger equation

$$\hat{H}_{ion}\Theta_a(\vec{R}, \vec{r}_c; \vec{r}) = U_a(\vec{r})\Theta_a(\vec{R}, \vec{r}_c; \vec{r}) \tag{2.6}$$

where Θ_a and U_a represent the wavefunction and ion energy of the parent ion at state a, respectively. Here $\vec{R}$ and $\vec{r}_c$ denote the nuclear coordinate and the coordinates of the core electrons, respectively, while $\vec{r}$ denotes the coordinate of the Rydberg electron. Notice that both Θ_a and U_a depends on the Rydberg electron coordinate $\vec{r}$ parametrically. The total wavefunction Ψ is expanded in terms of Θ_a.

$$\Psi = \sum_a \Phi_a(\vec{r})\Theta_a(\vec{R}, \vec{r}_c; \vec{r}) \tag{2.7}$$

Substituting Eq. (2.7) into the Schrödinger equation, multiplying Θ_b^* on the equation, integrating over the ionic coordinates, and neglecting the terms involving $\hat{H}'_{IBO}$, we obtain

$$(\hat{T}_e + U_b)\Phi_{bm} = E_{bm}\Phi_{bm} \tag{2.8}$$

and

$$\Psi_{bm} = \Phi_{bm}\Theta_b \tag{2.9}$$

Here m denotes the quantum numbers to specify the Rydberg electronic state. We shall denote the ionic wavefunction in the core electronic state c and rovibrational state w as Θ_{cw}; i.e., $b = cw$, and represent the corresponding Rydberg electronic wavefunction by Φ_{cwm}. From Eqs. (2.6) and (2.8), we can see that the eigenvalue U_b of ionic Schrödinger equation serves as the potential energy of the electronic Schrödinger equation. It can also be interpreted that the Rydberg electron is moving on the potential energy surface provided by the ion core in the rovibronic state cw.

Consider a molecule containing $n-1$ electrons in the core and one electron in the high Rydberg state (denoted as the electron n). The ionic Hamiltonian can be expressed as

$$\hat{H}_{ion} = -\frac{\hbar^2}{2m_e}\sum_{i=1}^{n-1}\nabla_i^2 + \hat{T}_N + V \tag{2.10}$$

where $\hat{T}_N$ is the kinetic energy operator of the nuclei. Next, we can separate the interactions containing the electron n from V

$$V = V_{ion} + \sum_{i=1}^{n-1}\frac{e^2}{r_{n,i}} - \sum_\alpha \frac{Z_\alpha e^2}{r_{n,\alpha}} \equiv V_{ion} + V' \tag{2.11}$$

where i represents the i-th electron in the ion core, and α refers to αth nucleus. V' can be approximated by the multipole expansion.

$$\begin{aligned} V' &= -\frac{e^2}{r_n} + \left[\sum_{i=1}^{n-1}\frac{e^2(\vec{r}_n\cdot\vec{r}_i)}{r_n^3} - \sum_\alpha \frac{Z_\alpha e^2(\vec{r}_n\cdot\vec{R}_\alpha)}{r_n^3}\right] \\ &\quad + \left\{\sum_{i=1}^{n-1}\frac{e^2}{2}\left[\frac{3(\vec{r}_n\cdot\vec{r}_i)^2}{r_n^5} - \frac{r_i^2}{r_n^3}\right] - \sum_\alpha \frac{Z_\alpha e^2}{2}\left[\frac{3(\vec{r}_n\cdot\vec{R}_\alpha)^2}{r_n^5} - \frac{R_\alpha^2}{r_n^3}\right]\right\} + \cdots \\ &\equiv -\frac{e^2}{r_n} + V'_d + V'_q + \cdots \end{aligned} \tag{2.12}$$

where V'_d denotes the dipole interaction and V'_q the quadrupole interaction, and so on. Neglecting the higher order interactions, we obtain the zeroth-order wavefunctions of the ion core and the Rydberg electron. That is, Eqs. (2.6) and (2.8) can be expressed as

$$\hat{H}^0_{ion}\Theta^0_{cw}(\vec{R}, \vec{r}_c) = U^0_{cw}\Theta^0_{cw}(\vec{R}, \vec{r}_c) \tag{2.13}$$

$$\left(\hat{T}_e - \frac{e^2}{r_n}\right)\Phi^0_m(\vec{r}_n) = \varepsilon^0_m\Phi^0_m(\vec{r}_n) \tag{2.14}$$

We see that the solution of Eq. (2.13) is the wavefunction of a bare ion, which can be calculated with the conventional quantum chemistry methods, while the solution of Eq. (2.14) is the hydrogen atom wavefunction. Therefore, similar to the conventional hydrogenic wavefunction [25], the wavefunction $\Phi^0_{nlm} = R_{nl}(r)Y_{lm}(\theta, \phi)$

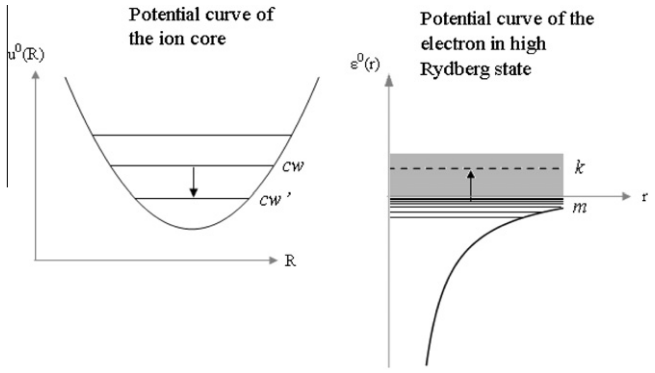

Fig. 1. The schematic plot of vibrational autoionization based on the model of IBOA. During the autoionization $cwm \rightarrow cw'k$, the ion core would relax from a vibrationally excited state cw to a lower state cw', while the electron in the high Rydberg state m would autoionize to the continuum state k.

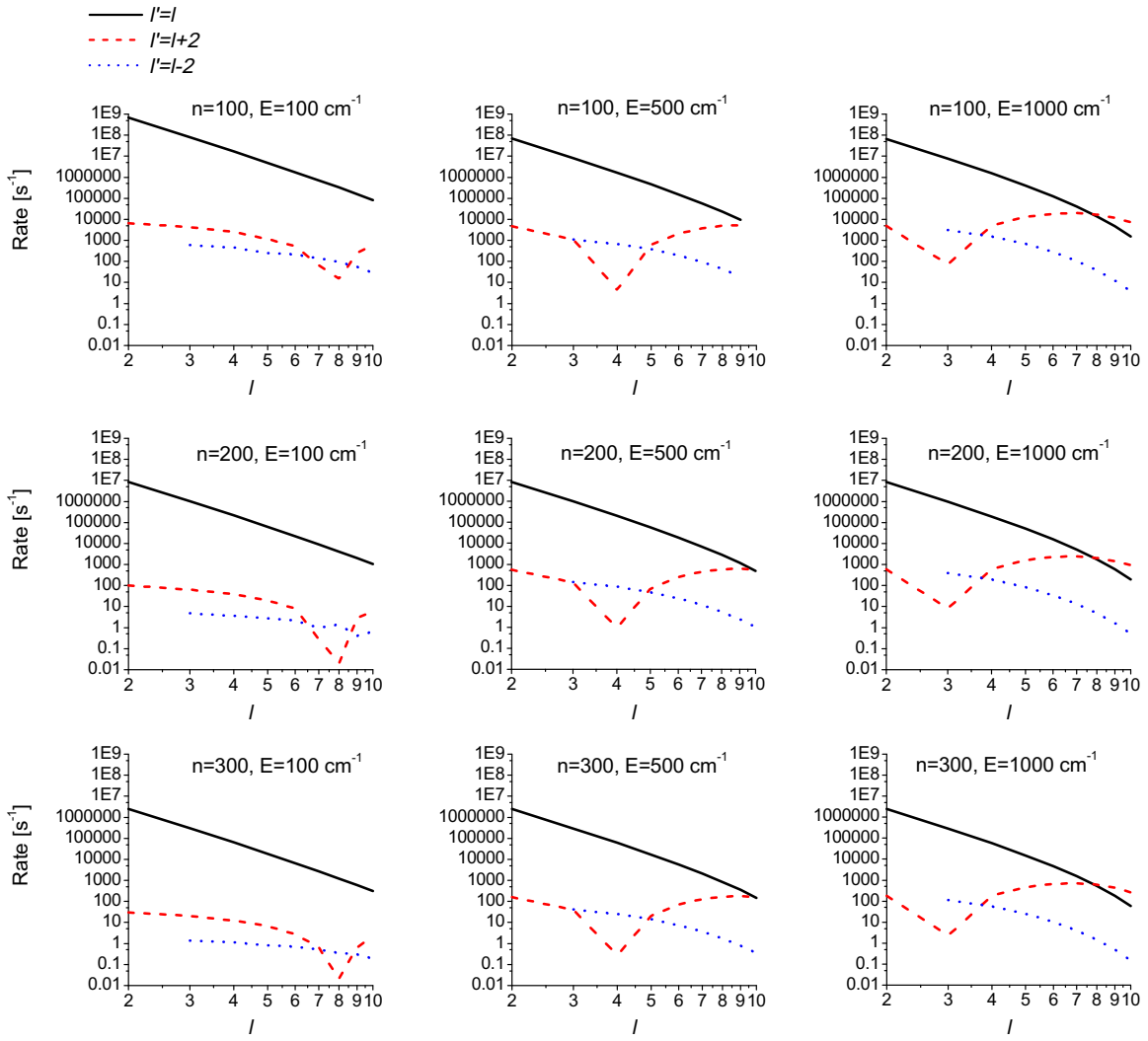

Fig. 2. The rovibrational autoionization rate constants of H_2 with transition $(v^+ = 1, N^+ = 0) \rightarrow (v^{+'} = 0, N^{+'} = 2)$ for $l' = l$, $l' = l + 2$, and $l' = l - 2$. The left panel is for the continuum-state energy of 100 cm^{-1}; the middle panel is for the continuum-state energy of 500 cm^{-1}, and the right panel is for the energy of 1000 cm^{-1}.

with the quantum numbers *nlm* can be used to describe the bound electron, while *klm* can be used to describe the free electron.

To solve Eq. (2.13), we can use Born–Oppenheimer approximation and the ionic wavefunction Θ_{cw} can be separated as the core electronic wavefunction φ_c and the nuclear wavefunction ψ_{cw}. That is,

$$\hat{H}^0_{ion} = \hat{H}^0_e + \hat{T}_N \tag{2.15}$$

$$\hat{H}^0_e \varphi^0_c = u^0_c \varphi^0_c \tag{2.16}$$

$$(\hat{T}_N + u^0_c)\psi^0_{cw} = U^0_{cw}\psi^0_{cw} \tag{2.17}$$

and

$$\Theta^0_{cw} = \varphi^0_c \psi^0_{cw} \tag{2.18}$$

where $\hat{H}^0_e$ denotes the Hamiltonian of the core electrons after subtracting the nuclear kinetic energy operator $\hat{T}_N$ from $\hat{H}^0_{ion}$. In the case of diatomic molecules, the zeroth-order nuclear wavefunction ψ^0_{cw} can be expressed in spherical coordinates $\vec{R} = (R, \Theta, \Phi)$ as

$$\psi^0_{cv^+N^+M^+_N} = \chi_{cv^+}(R) Y_{N^+M^+_N}(\Theta, \Phi) \tag{2.19}$$

where χ_{cv^+} denotes the vibrational wavefunction and $Y_{N^+M^+_N}$ denotes the rotational wavefunction with respect to the electronic state *c* of the ion core. Here $w = v^+N^+M^+_N$ denote the vibration and rotation quantum numbers.

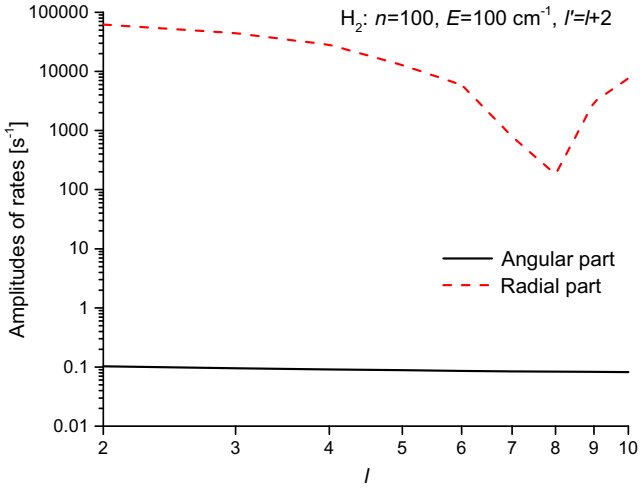

Fig. 3. The angular and radial dependent parts of the rovibrational autoionization rate constants for Rydberg state $(n = 100, l)$ of H_2 with transition $(v^+ = 1, N^+ = 0) \rightarrow (v^{+'} = 0, N^{+'} = 2)$ for $l' = l + 2$. The continuum-state energy is 100 cm^{-1}.

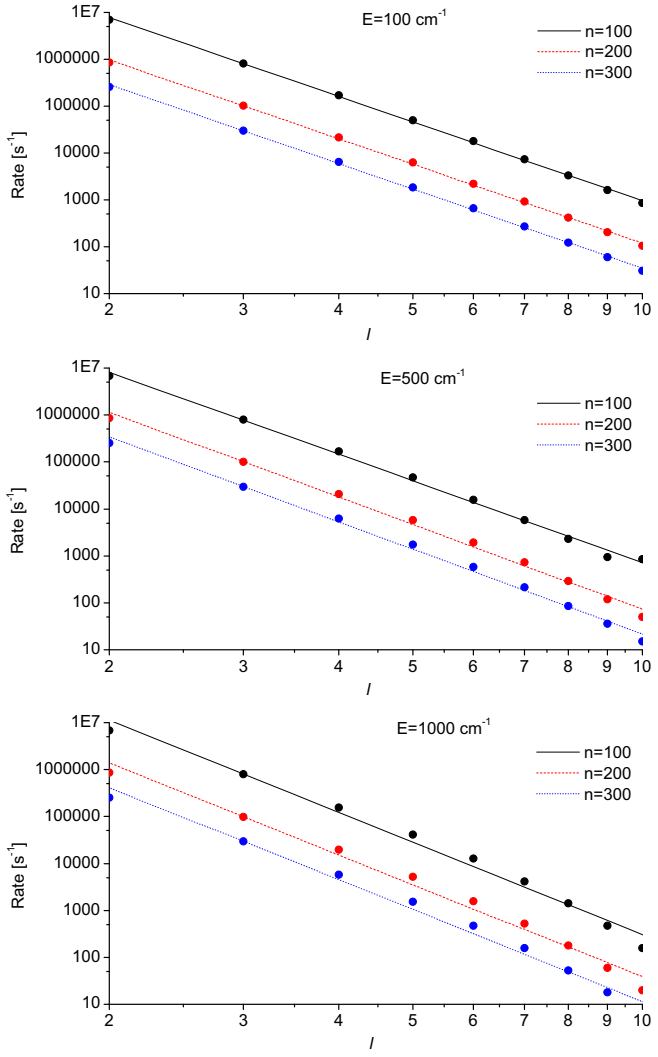

Fig. 4. The autoionization rate constants for Rydberg state ($n = 100$, l) of H_2 with transition $(v^+ = 1, N^+ = 0) \rightarrow (v^{+\prime} = 0, N^{+\prime} = 2)$ for $l' = l$, based on the quadrupole interaction. The three panels are for the continuum-state energy of 100, 500, and 1000 cm^{-1}, respectively. The calculated rate constants are marked by symbols for each n, l and the lines represent the data obtained from the scaling law.

For a homonuclear diatomic molecule, the first-order energy correction of the dipole interaction is zero, so we shall perform the first-order correction of the quadrupole term. It follows that

$$u_c^{(1)} = \langle \varphi_c^0 | V_q' | \varphi_c^0 \rangle \tag{2.20}$$

Performing the integration with respect to the core electronic coordinates R_c, we can obtain the conventional expression by using quadrupole moment Q as functions of the nuclear coordinate $\vec{R}$.

$$u_c^{(1)} = -e\frac{Q_c(R)}{r^3}\left[\frac{4\pi}{5}\sum_{\bar{m}=-2}^{2} Y_{2\bar{m}}(\theta,\phi)Y_{2\bar{m}}^*(\Theta,\Phi)\right] \tag{2.21}$$

where the first spherical harmonics depends on the coordinate of the Rydberg electron, and the second one depends on that of the ion core.

The basic concept of autoionization can be understood by using the diagram in Fig. 1, In the high Rydberg state, the electron behaves like a hydrogenic electron, and the core like a bare ion. The interaction between them is very week, so we can form two independent systems, as shown in the zeroth-order Hamiltonian. The molecule was first excited to a vibrationally or rotationally excited state with one electron in the high Rydberg state. Due to the interaction within the molecule, the excited core would release its energy and transfer the energy to the Rydberg electron, thus yielding ionization. With this understanding, we can calculate the corresponding transition rate.

To derive the expression of the autoionization rate, we need to include the neglected term in Eq. (2.8), denoted as $\hat{H}'_{IBO}$; in other words, the radiationless transition is interpreted as the breakdown of the IBOA [20]. Therefore, the autoionization rate constant is

$$W_{(cwm\rightarrow cw'k)} = \frac{2\pi}{\hbar}\left|\left\langle \Psi_{cw'k}\middle|\hat{H}'_{IBO}\middle|\Psi_{cwm}\right\rangle\right|^2 \rho(E_k) \tag{2.22}$$

where $\rho(E_k)$ is the density of states for the ionized electron of energy E_k and

$$\left\langle \Psi_{cw'k}\middle|\hat{H}'_{IBO}\middle|\Psi_{cwm}\right\rangle = -\frac{\hbar^2}{2m_e}\left(2\langle\Phi_{cw'k}|\langle\Theta_{cw'}|\nabla_e\Theta_{cw}\rangle\cdot|\nabla_e\Phi_{cwm}\rangle + \langle\Phi_{cw'k}|\left\langle\Theta_{cw'}\middle|\nabla_e^2\Theta_{cw}\right\rangle\middle|\Phi_{cwm}\right\rangle\right) \tag{2.23}$$

Notice that

$$\begin{aligned}\langle\Theta_{cv^{+\prime}N^{+\prime}M_N^{+\prime}}|\nabla_e|\Theta_{cv^+N^+M_N^+}\rangle &= \frac{\left\langle\Theta^0_{cv^{+\prime}N^{+\prime}M_N^{+\prime}}|\nabla_e V_q'|\Theta^0_{cv^+N^+M_N^+}\right\rangle}{U^0_{cv^+N^+}-U^0_{cv^{+\prime}N^{+\prime}}}\\ &= -e\frac{\langle\chi_{cv^{+\prime}}|Q_c|\chi_{cv^+}\rangle}{U^0_{cv^+N^+}-U^0_{cv^{+\prime}N^{+\prime}}}\\ &\times\left\{\frac{4\pi}{5}\sum_{\bar{m}=-2}^{2}\left\langle Y_{N^{+\prime}M_N^{+\prime}}\middle|Y^*_{2\bar{m}}\middle|Y_{N^+M_N^+}\right\rangle\nabla_e\left[\frac{Y_{2\bar{m}}(\theta,\phi)}{r^3}\right]\right\}\end{aligned} \tag{2.24}$$

$$\langle\Theta_{cv^{+\prime}N^{+\prime}M_N^{+\prime}}|\nabla_e^2|\Theta_{cv^+N^+M_N^+}\rangle = \frac{\langle\Theta^0_{cv^{+\prime}N^{+\prime}M_N^{+\prime}}|\nabla_e^2 V_q'|\Theta^0_{cv^+N^+M_N^+}\rangle}{U^0_{cv^+N^+}-U^0_{cv^{+\prime}N^{+\prime}}} = 0$$

Here $w' = v^{+\prime}N^{+\prime}M_N^{+\prime}$, $k = kl'm'$, $w = v^+N^+M_N^+$ and $m = nlm$, respectively. The second term is vanishing because the electronic part of the quadrupole interaction V_q' is a solution of the Laplace equation. Finally we obtain

$$\begin{aligned}&\langle kl'v^{+\prime}N^{+\prime}JM_J\left|\hat{H}'_{IBOA}\right|nlv^+N^+JM_J\rangle\\ &= -\frac{\hbar^2}{m_e}\frac{(-e)}{U^0_{cv^+N^+}-U^0_{cv^{+\prime}N^{+\prime}}}\langle\chi_{cv^{+\prime}}|Q_c(R)|\chi_{cv^+}\rangle\\ &\times\left[D_{l',l}\langle R_{kl'}|r^{-5}|R_{nl}\rangle - 3\langle R_{kl'}|r^{-4}|\frac{dR_{nl}}{dr}>\right]\\ &\times g(l',N^{+\prime},J',M'_J;l,N^+,J,M_J)\end{aligned} \tag{2.25}$$

where nl and kl' represent the quantum numbers of discrete states and that of continuum states of the ZEKE electron, respectively, and $D_{l,l} = 3$, $D_{l+2,l} = -2l$, and $D_{l-2,l} = 2(l+1)$ (see Appendix). The angular matrix element g is given in [26–27].

In Eq. (2.25), there are three matrix elements to be calculated. The first matrix element contains the quadrupole moment of the ion core, which is a function of internuclear distance R. It is responsible for the vibrational transition. As the propensity rule of vibrational autoionization, the magnitude of the corresponding transition rate would decrease rapidly as Δv increases [28,29]. The second one is the radial integral of the Rydberg electron, and it describes the transition from an electronic bound state to the continuum. In this section, we employed the recursion relation of associated Laguerre polynomial and performed the numerical integration to obtain the value of this matrix element. The last one involves the angular momentum for both electronic and nuclear rotation motions. Due to the symmetry of spherical harmonics, the allowed transitions should obey $\Delta l = 0,\pm2$ and $\Delta N^+ = 0,\pm2$. In addition, the projection quantum numbers m and M_N^+ are summed for the coupling between the electronic orbital angular momentum

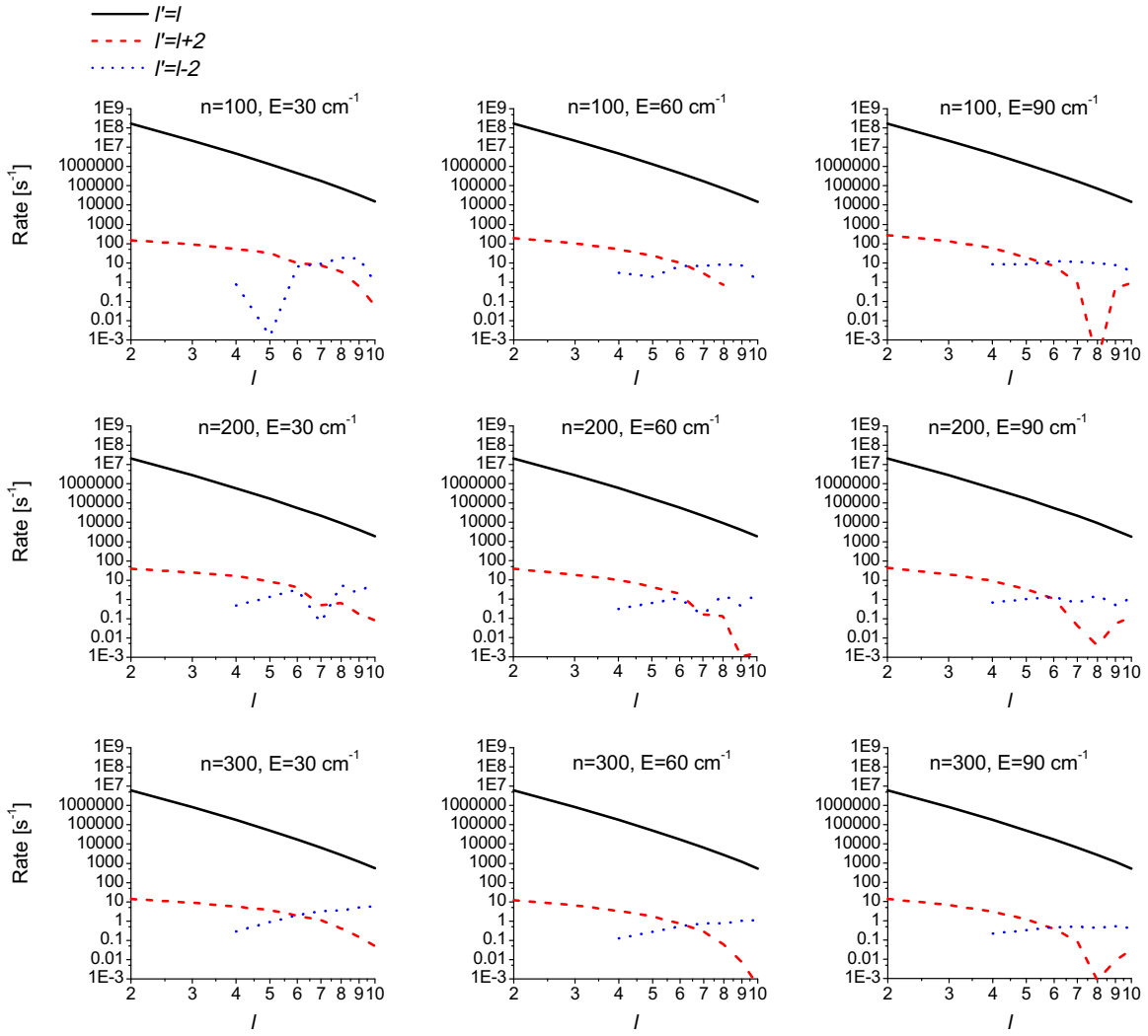

Fig. 5. The rotational autoionization rate constants of N_2 with transition $\{nl,\ v^+=0, N^+=10, J=10M_J\} \rightarrow \{kl,\ v^{+'}=0, N^{+'}=8, J=10M_J\}$ for $l'=l$, $l'=l+2$, and $l'=l-2$. The left panel is for the continuum-state energy of 30 cm^{-1}; the middle panel is for the continuum-state energy of 60 cm^{-1}, and the right panel is for the energy of 90 cm^{-1}.

l and the core rotational angular momentum N^+. Then, we have the total angular momentum J and its projection quantum number M_J. Due to the Kronecker delta, J and M_J are constant upon the transition. The selection rules and propensity rule of this formulation are in agreement with the previous studies of autoionization based on the multipole interaction [27] and the multichannel quantum defect theory [30,31].

3. Results and discussion

Here we calculate the autoionization rate of H_2 for the transition among different rotational and vibrational states with transition $\{nl;\ v^+N^+;JM_J\} \rightarrow \{kl';\ v^{+'}N^{+'};JM_J\}$. In the following, we will consider the transitions for different n, l and energy of the unbound state; the related transition for vibrational and rotational states is $(v^+=1, N^+=0) \rightarrow (v^{+'}=0, N^{+'}=2)$. As shown in Fig. 1, there is an energy restriction for autoionization. Nevertheless, in order to conveniently analyze the relation between the transition rate and the corresponding quantum numbers, as well as the energy dependence, we first release this restriction. The actual observations, of course, correspond to specific data points satisfying the energy conservation restriction.

The numerical results calculated using Eq. (2.25) for H_2 are given in Fig. 2. If we specify the quantum numbers n and k, there are three possibilities of the final l' which obey the selection rule. First, in the case of $l'=l$, we can see that the rate decreases rapidly with increasing l. For example, the corresponding rates of $n=100$ can range from 10^3 to 10^9 s^{-1}. This behavior can be understood by the property of the hydrogenic wavefunction [25]. That is, the states at low l would have larger core penetration as well as stronger interaction, and thus the rate would decrease as l increases. Likewise, the related rate would decrease as n increases due to the weak interaction between the Rydberg electron and ion core. As for the k dependence, we found that the transition rates for low-l states are relatively invariant to the influence of k. However, those of high-l states have stronger energy dependence as the energy increases.

Compared with the transitions of $l'=l$, those of $l'=l+2$ and $l'=l-2$ are relatively slow. However, for the energy of 1000 cm^{-1}, the transitions of $l'=l+2$ would compete with those of $l'=l$ at larger l ($l>8$). Besides, from Fig. 2, we can see that there is no obvious tendency for these two cases. For $l'=l-2$, the rate would decrease with increasing l. On the other hand, for $l'=l+2$, we can find a dip for a specific l in each plot. For both cases, the magnitudes of the autoionization rates are more sensitive to the energy than $l'=l$. To further study the irregular l dependence, we separate the angular and radial dependent parts in Eq. (2.25), where the angular part distribution is given by $|g(l', N^{+'}, J',$

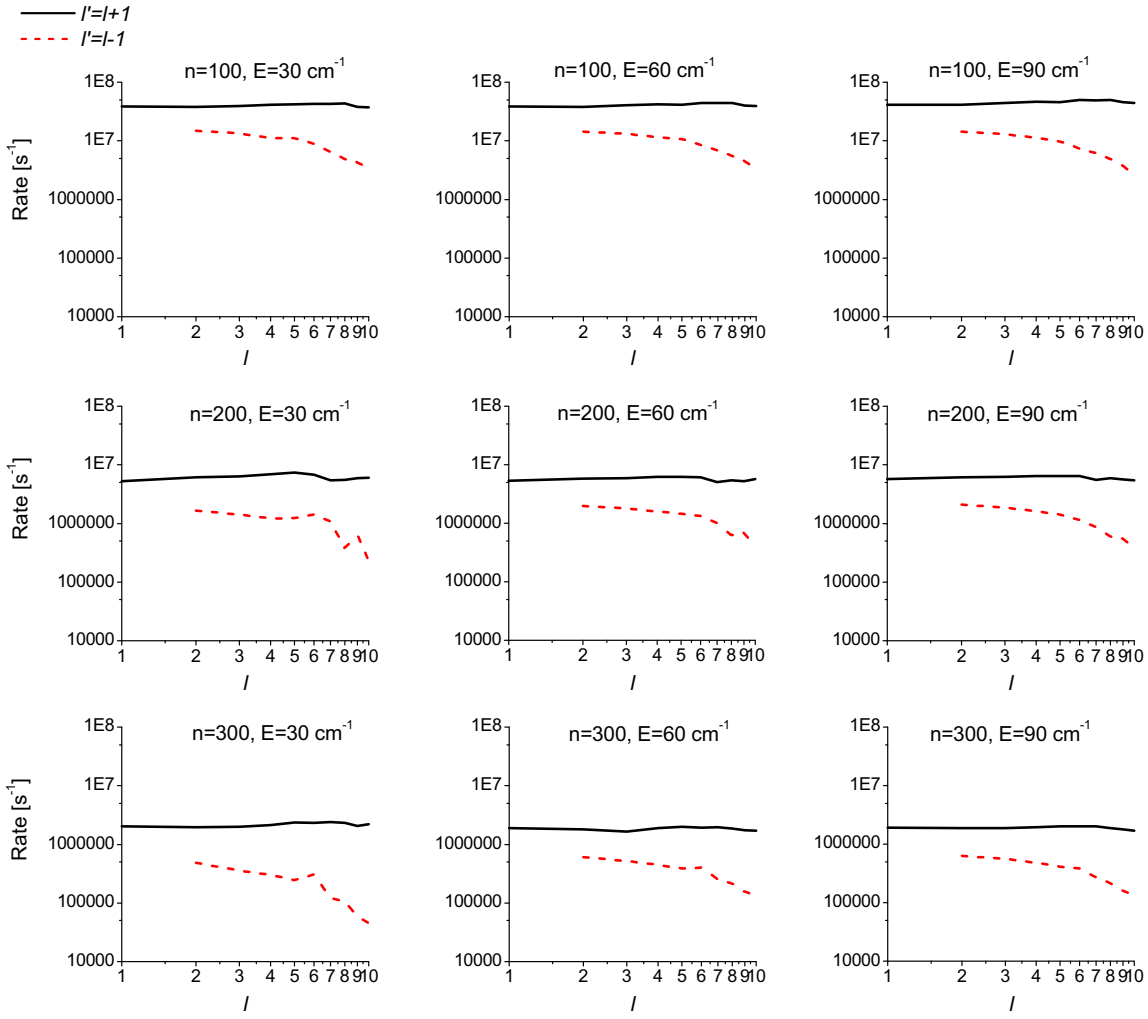

Fig. 6. The rotational autoionization rate constants of HCl with transition $\{nl,\ v^+ = 0, N^+ = 0\} \rightarrow \{kl \pm 1,\ v^{+'} = 0, N^{+'} = 1\}$ for $l' = l + 1$ and $l' = l - 1$ in terms of the dipole interaction. The left panel is for the continuum-state energy of 30 cm^{-1}; the middle panel is for the continuum-state energy of 60 cm^{-1}, and the right panel is for the energy of 90 cm^{-1}.

$M'_J; l, N^+, J, M_J)|^2$ which is dimensionless, and the radial part is the rest contribution. We see in Fig. 3 that the l dependence of the transition rate mainly comes from the radial part. The subtle interplay of the radial wavefunctions yields irregular integrands and subsequently the irregular l dependence.

From Fig. 2, it is clear that the transition of $l' = l$ shows a regular power law dependence of l. Using a nonlinear modelling, we obtain the scaling law for the autoionization rate as

$$rate = 3.61 \times 10^{15} n^{-3} l^{-5.3} s^{-1} \tag{3.1}$$

The n^3 law is consistent with that obtained from the asymptotic wavefunction of high Rydberg state [27–31]. The comparison between the calculated data and the fitting curves is shown in Fig. 4.

In Fig. 4, we can see the numerical results agree well with the estimation of the scaling law for the low energy case. In Eq. (3.1), the scaling law is independent of the energy of the continuum state, but it still works well for the low-l transitions when the energy is relatively high. For instance, it can effectively predict the rate up to $l = 5$ for the energy of 1000 cm^{-1}. On the other hand, for the transitions $l' = l \pm 2$, we cannot derive a scaling law of the transition rate due to the irregular dependence on l. Nevertheless, for most cases, $l' = l$ is the most probable transition, so we can neglect the contribution of $l' = l \pm 2$ transitions. In this sense, this scaling law is quite useful to gain an approximate magnitude of the autoionization rate.

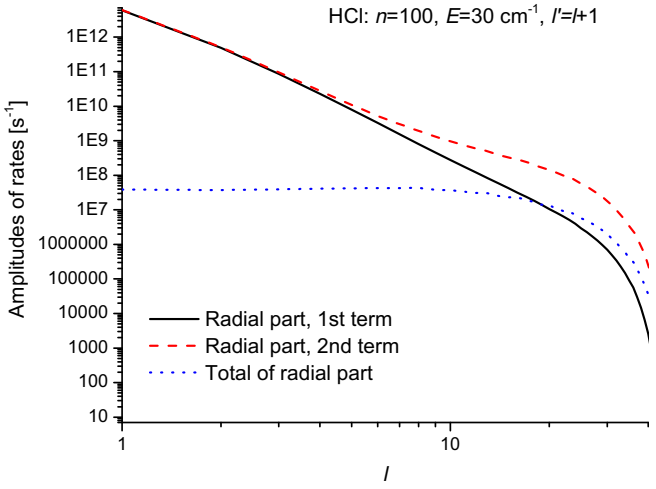

Fig. 7. Comparisons of the contribution of the two terms in the radial dependent part of Eq. (2.25) for the rotational autoionization rate constants of HCl with transition $\{nl,\ v^+ = 0, N^+ = 0\} \rightarrow \{kl + 1,\ v^{+'} = 0, N^{+'} = 1\}$ in terms of the dipole interaction. The continuum-state energy of 30 cm^{-1}.

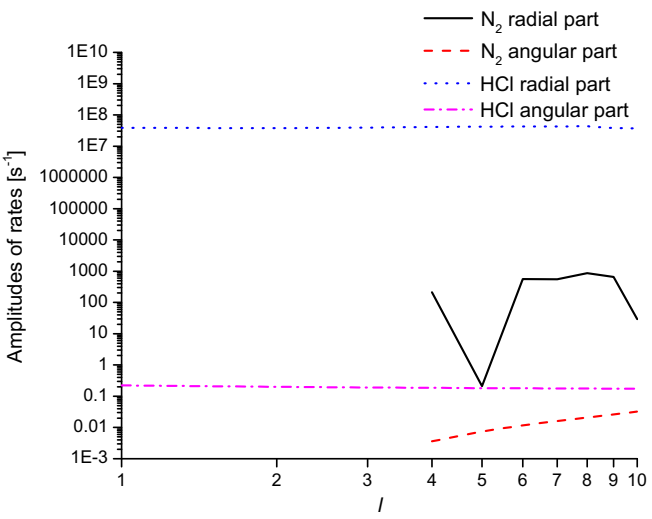

Fig. 8. Comparisons of the angular and radial dependent parts of the HCl $\{nl,\ v^+=0,\ N^+=0\}\rightarrow\{kl+1,\ v^{+'}=0,\ N^{+'}=1\}$ and N_2 $\{nl,\ v^+=0,\ N^+=10, J=10M_J\}\rightarrow\{kl,\ v^{+'}=0,\ N^{+'}=8, J=10M_J\}$. Here we use $E=30\ \mathrm{cm}^{-1}$ and $n=100$ for both molecules HCl and N_2.

Next, we consider the rotational autoionization of N_2. The bond length (2.175 au) and the quadrupole momentum (1.974 au) of N_2^+ were calculated by the Gaussian package [32] suite with the UCCSD/aug-cc-pVDZ level of theory. Here we consider the transition $\{nl,\ v^+=0,\ N^+=10, J=10M_J\}\rightarrow\{kl,\ v^{+'}=0,\ N^{+'}=8,\ J=10M_J\}$. The resulting autoionization rates are shown in Fig. 5. We can see that the magnitude of the autoionization rate decreases significantly with increases in l. Also, the rates of $l'=l+2$ and $l'=l-2$ are much slower than those of $l'=l$. Using the nonlinear regression, we find that the transition of $l'=l$ follows a regular power law dependence of l. The scaling law is

$$rate=6.50\times10^{15}n^{-3}l^{-5.3}\times0.9^{(N^+-2)}s^{-1} \tag{3.2}$$

For heteronuclear diatomic molecules, the dipole interaction has to be considered. For example, here we consider the rotational autoionization of HCl molecule. The bond length (2.514 au) and the dipole momentum (0.669 au) of HCl^+ were calculated by the Gaussian package [32] suite with the UCCSD/aug-cc-pVDZ level of theory. The transition we consider is $\{nl,\ v^+=0,\ N^+=0\}\rightarrow\{kl\pm1,\ v^{+'}=0,\ N^{+'}=1\}$. The autoionization rates are shown in Fig. 6. It is found that the magnitude of the autoionization of $l'=l+1$ is larger than that of $l'=l-1$, and almost independent on l and E. The autoionization of $l'=l-1$ also shows same tendency, but dependence on l' is roughly proportional to $l'^{-0.7}$. The n^3 law is consistent with the previous autoionization results of Eqs. (3.1) and (3.2). The almost l independency of the $l'=l+1$ transition deserves further analysis. First, the main contribution in Eq. (2.25) comes from the radial part, which contains two terms. We thus study the l dependence from the two terms separately. In Fig. 7 we show the results. We see clearly that it is due to the cancellation of the delicate interplay of the two radial terms that the final transition rates become almost l independent. Notice that similar trends have been observed before [33].

In order to see the difference of the autoionization rates of HCl and N_2 we divide autoionization rates into the angular and radial dependent parts. In Fig. 8 magnitudes of angular and radial dependent parts of the autoionization rates are plotted. Here we use $E=30\ \mathrm{cm}^{-1}$ and $n=100$ for both molecules HCl and N_2, and consider the same transitions as they have appeared in this section, HCl $\{nl,\ v^+=0,\ N^+=0\}\rightarrow\{kl+1,\ v^{+'}=0,\ N^{+'}=1\}$ and $N_2\{nl,\ v^+=0,\ N^+=10,\ J=10M_J\}\rightarrow\{kl,\ v^{+'}=0,\ N^{+'}=8,\ J=10M_J\}$. From this figure we find that the angular parts for both molecules are almost flat and independent on l. The l dependence of the radial part of HCl is also very week, however the radial part of N_2 molecule decreases rapidly with increasing l. It is considered that l dependence of the angular parts of the dipole and quadrupole moments are not very different, on the other hand l dependence of the radial parts of them show a large difference. We conclude that whole tendency of l dependence of the autoionization rates are determined from the radial parts of diatomic molecules.

Finally, the influence of Stark-mixing due to the stray field has been found to be crucial and needs to be included in our discussion of autoionization rates. Chupka has proposed that the optically accessible populations in low-l states would transfer to high-l states, resulting in reduction of core penetration [34], and in previous studies we have numerically demonstrated this [17,18]. That is, the low-l states contributing significantly near the ion core experience a stronger interaction with the core. Hence, electrons in low-l states would quickly disappear through various relaxation processes such as autoionization. From the scaling laws we obtain in the present work, we can see that the transition rate decreases significantly as l increases for both rotational and vibrational autoionizations. Consequently, after a long period of delay time, only the states with higher l would survive and be observed in ZEKE experiments. In the case of $l=3$, the lifetime of rotational autoionization from high Rydberg state is about 1 microsecond, and that of vibrational autoionization is about one order of magnitude smaller. The autoionization in this range might be observed in the ZEKE experiments with comparable delay time.

4. Conclusion

In this paper we have derived the master equation for autoionization dynamics, which is the main radiationless process involved in ZEKE spectroscopy. The inverse Born–Oppenheimer approximation (IBOA) has been employed to establish a proper basis set for high Rydberg states. With this scheme autoionization is interpreted as the breakdown of the IBOA and the rate constants can be systematically calculated. We apply this formulation to calculate the vibrational autoionization rate constants of H_2 and rotational autoionization rate constants of N_2 and HCl. These calculated data can be summarized as the scaling laws with respect to the quantum numbers and can be very useful for quantitatively studying the intricate dynamics in ZEKE spectroscopy.

Acknowledgements

This work is partly supported by the NSC of ROC and CQSE of NTU 10R80914-1.

Appendix A. Derivation of the angular matrix elements

$$\begin{aligned}
&\left\langle Y_{l_1,m_1}\left|\frac{\partial Y_{l_2,m_2}}{\partial\theta}\right|\frac{\partial Y_{l_3,m_3}}{\partial\theta}\right\rangle+\left\langle Y_{l_1,m_1}\left|\frac{1}{\sin\theta}\frac{\partial Y_{l_2,m_2}}{\partial\phi}\right|\frac{1}{\sin\theta}\frac{\partial Y_{l_3,m_3}}{\partial\phi}\right\rangle\\
&=-\left\langle Y_{l_1,m_1}\left|\hat r\times\hat L Y_{l_2,m_2}\right|\hat r\times\hat L Y_{l_3,m_3}\right\rangle=-\left\langle Y_{l_1,m_1}\left|\hat L Y_{l_2,m_2}\right|\hat L Y_{l_3,m_3}\right\rangle\\
&=-\frac{1}{2}\left\langle Y_{l_1,m_1}\left|\hat L_+ Y_{l_2,m_2}\right|\hat L_- Y_{l_3,m_3}\right\rangle-\frac{1}{2}\left\langle Y_{l_1,m_1}\left|\hat L_- Y_{l_2,m_2}\right|\hat L_+ Y_{l_3,m_3}\right\rangle\\
&\quad-m_2m_3\left\langle Y_{l_1,m_1}\middle|Y_{l_2,m_2}\middle|Y_{l_3,m_3}\right\rangle\\
&=-\frac{1}{2}\left[\sqrt{(l_2-m_2)(l_2+m_2+1)(l_3+m_3)(l_3-m_3+1)}\right.\\
&\quad\times\left\langle Y_{l_1,m_1}\middle|Y_{l_2,m_2+1}\middle|Y_{l_3,m_3-1}\right\rangle\\
&\quad\left.+\sqrt{(l_2+m_2)(l_2-m_2+1)(l_3-m_3)(l_3+m_3+1)}\right.\\
&\quad\times\left\langle Y_{l_1,m_1}\middle|Y_{l_2,m_2-1}\middle|Y_{l_3,m_3+1}\right\rangle+2m_2m_3\left\langle Y_{l_1,m_1}\middle|Y_{l_2,m_2}\middle|Y_{l_3,m_3}\right\rangle
\end{aligned}$$

Using the 3-j symbol, we have

$$
\begin{aligned}
&[l_1(l_1+1)-l_2(l_2+1)-l_3(l_3+1)-2m_2m_3]\times\begin{pmatrix} l_1 & l_2 & l_3 \\ m_1 & m_2 & m_3 \end{pmatrix} \\
&=\sqrt{(l_2-m_2)(l_2+m_2+1)(l_3+m_3)(l_3-m_3+1)} \\
&\quad\times\begin{pmatrix} l_1 & l_2 & l_3 \\ m_1 & m_2+1 & m_3-1 \end{pmatrix} \\
&\quad+\sqrt{(l_2+m_2)(l_2-m_2+1)(l_3-m_3)(l_3+m_3+1)}\begin{pmatrix} l_1 & l_2 & l_3 \\ m_1 & m_2-1 & m_3+1 \end{pmatrix}
\end{aligned}
$$

Thus we obtain

$$
\begin{aligned}
&\left\langle Y_{l_1,m_1}\left|\frac{\partial Y_{l_2,m_2}}{\partial\theta}\right|\frac{\partial Y_{l_3,m_3}}{\partial\theta}\right\rangle+\left\langle Y_{l_1,m_1}\left|\frac{1}{\sin\theta}\frac{\partial Y_{l_2,m_2}}{\partial\phi}\right|\frac{1}{\sin\theta}\frac{\partial Y_{l_3,m_3}}{\partial\phi}\right\rangle \\
&\quad=-\frac{1}{2}[l_1(l_1+1)-l_2(l_2+1)-l_3(l_3+1)]\langle Y_{l_1,m_1}|Y_{l_2,m_2}|Y_{l_3,m_3}\rangle
\end{aligned}
$$

For the quadrupole interaction, $l_2 = 2$, and we obtain $D_{l,l} = 3$, $D_{l+2,l} = -2l$, $D_{l-2,l} = 2(l+1)$.

References

[1] K. Müller-Dethlefs, M. Sander, E.W. Schlag, Chem. Phys. Lett. 112 (1984) 291.
[2] E.W. Schlag, ZEKE Spectroscopy, Cambridge University Press, Cambridge, 1998.
[3] M.C.R. Cockett, Chem. Soc. Rev. 34 (2005) 935.
[4] S. Willitsch, A. Wuest, F. Merkt, Chimia 58 (2004) 281.
[5] K. Müller-Dethlefs, E.W. Schlag, Ann. Rev. Phys. Chem. 42 (1991) 109.
[6] F. Merkt, Annu. Rev. Phys. Chem. 48 (1997) 673.
[7] C.Y. Ng, Annu. Rev. Phys. Chem. 53 (2002) 101.
[8] T. Wright, Annu. Rep. Prog. Chem. Sect. C 98 (2002) 375.
[9] H.J. Neusser, H. Krause, Chem. Rev. 94 (1994) 1829.
[10] C.E.H. Dessent, K. Müller-Dethlefs, Chem. Rev. 100 (2000) 3999.
[11] L. Zhu, P. Johnson, J. Chem. Phys. 94 (1991) 5769.
[12] R.C. Shiell, X.K. Hu, Q.C.J. Hu, J.W. Hepburn, Faraday Discu. 115 (2000) 331.
[13] L. Schneider, W. Meier, E. Wrede, K.H. Welge, M.N.R. Ashfold, C.M. Western, J. Chem. Phys. 92 (1990) 7027.
[14] F. Merkt, T.P. Softley, Int. Rev. Phys. Chem. 12 (1993) 205.
[15] K. Müller-Dethlefs, O. Dopfer, Chem. Rev. 94 (1994) 1845.
[16] F. Remacle, R.D. Levine, Int. J. Quan. Chem. 67 (1998) 85.
[17] S.D. Chao, M. Hayashi, S.H. Lin, E.W. Schlag, J. Phys. B 32 (1998) 2007.
[18] S.D. Chao, M. Hayashi, S.H. Lin, E.W. Schlag, J. Chin. Chem. Soc. 45 (1998) 491.
[19] S.D. Chao, H.Y. Peng, J. Mol. Spec. 247 (2008) 30.
[20] Y.H. Wang, H. Mineo, S.D. Chao, H.L. Selzle, H.J. Neusser, E.W. Schlag, Y. Teranishi, S.H. Lin, J. Chem. Phys. 134 (2011) 064316.
[21] T.P. Softley, Int. Rev. Phys. Chem. 23 (2004) 1.
[22] Y.H. Wang, Y. Teranishi, H. Mineo, S.D. Chao, H.L. Selzle, H.J. Neusser, E.W. Schlag, S.H. Lin, Chem. Phys. Lett. 486 (2010) 104.
[23] S.H. Lin, R. Alden, R. Islampour, H. Ma, A.A. Villaeys, Density Matrix Method and Femtosecond Processes, World Scientific, Singapore, 1991.
[24] M.J.J. Vrakking, D.M. Villeneuve, A. Stolow, Phys. Rev. A 54 (1996) R37.
[25] H.A. Bethe, E.E. Salpeter, Quantum Mechanics of One- and Two-Electron Atom, Academic Press Inc., New York, 1957.
[26] M. Bixon, J. Jortner, Mol. Phys. 89 (1996) 373.
[27] E.E. Eyler, F.M. Pipkin, Phys. Rev. A 27 (1983) 2462.
[28] D.R. Bates, G. Poots, Proc. Phys. Soc. (London) A66 (1953) 784.
[29] R.S. Berry, J. Chem. Phys. 45 (1966) 1128.
[30] G. Herzberg, Ch. Jungen, J. Mol. Spectrosc. 41 (1972) 425.
[31] M. Raoult, Ch. Jungen, J. Chem. Phys. 74 (1981) 3388.
[32] M.J. Frisch, G.W. Trucks, H.B. Schlegel, et al., GAUSSIAN 03, Revision C.2, Gaussian, Inc., Pittsburgh PA, 2003.
[33] L. Ya Baranov, F. Remacle, R.D. Levine, Phys. Rev. A 54 (1996) 4789.
[34] W.A. Chupka, J. Chem. Phys. 98 (1993) 4520.